Journal of Membrane Science 460 (2014) 91–98

Contents lists available at ScienceDirect

Journal of Membrane Science

journal homepage: www.elsevier.com/locate/memsci

Fabrication of flexible, aligned carbon nanotube/polymer composite membranes by in-situ polymerization

Sangil Kim [a,*], Francesco Fornasiero [a], Hyung Gyu Park [b], Jung Bin In [c], Eric Meshot [a], Gabriel Giraldo [d], Michael Stadermann [a], Micha Fireman [e], Jerry Shan [d], Costas P. Grigoropoulos [c], Olgica Bakajin [e]

[a] Lawrence Livermore National Laboratory, Livermore, CA 94550, USA
[b] Department of Mechanical and Process Engineering, ETH Zurich, Zurich CH-8092, Switzerland
[c] Department of Mechanical Engineering, University of California Berkeley, Berkeley, CA 94720, USA
[d] Department of Mechanical and Aerospace Engineering, Rutgers University, NJ 08854, USA
[e] Porifera Inc., Hayward, CA 94545, USA

ARTICLE INFO

Article history:
Received 19 September 2013
Received in revised form
8 February 2014
Accepted 12 February 2014
Available online 19 February 2014

Keywords:
Carbon nanotubes
Nanocomposites
Membrane
Separations
Nanofluidics

ABSTRACT

Vertically aligned (VA) carbon nanotubes (CNTs) have shown orders of magnitude enhancement for gas and liquid flow compared to conventional mass transport theories. Flexible, large surface-area VACNT membranes may provide a cost-efficient solution to various separation processes such as water purification and gas separation. However, all the VACNT membranes produced so far suffer from rather small membrane area, long fabrication process, poor mechanical stability, local agglomeration of CNTs, and low CNT packing density. Here, we present flexible, VACNT/polymer composite membranes having relatively densely packed CNTs as the only mass transport paths. In order to prevent CNT condensation that could disturb CNT orientation during liquid phase processing, we developed a novel in-situ bulk polymerization method to prepare VACNT/polymer composite films. A VACNT array was infiltrated with styrene monomer with a certain amount of polystyrene–polybutadiene (PS–PB) copolymer that acts as a plasticizer. Indeed, micro-indentation measurements confirmed that the addition PS-b–PB copolymer into the matrix improved the elongation at break of the CNT/PS composite film. SEM images showed that well aligned CNTs were embedded in a high-density polymer matrix free of any macroscopic voids or structural defects. Measured fluid rates and selectivity for gas and liquid mixtures are consistent with CNT membranes produced with different methods. These CNTs/polymer composite membranes showed high gas and water permeability comparable to the other VACNT composite membranes, potentially enabling applications that may require membranes with high flux, flexibility and durability.

1. Introduction

Exceptional electrical, thermal, mechanical, and mass transport properties of CNTs [1–7] make the CNTs a promising nanoporous material for applications in membrane separation. One-dimensional graphitic nanochannel structure of CNTs is of particular interest as a building block for the next generation membranes [5,6,8–12]. Exciting predictions from molecular dynamics simulations have motivated fabrication of CNT membrane platforms to develop new membrane materials with extremely large gas or water permeation. Hummer et al. have found that water molecules could transport in a single-file configuration through narrow CNTs at ultrahigh rates due to molecular ordering and tight hydrogen bonding under extreme graphitic nanoconfinement [13]. Atomistic simulation studies by Sholl et al. have also predicted unprecedentedly large gas permeation and selectivity of CNTs due to their atomically smooth wall and preferential gas–wall interactions [14].

Several research groups have experimentally verified predictions of MD simulations by employing CNT membranes fabricated by different methods. Hinds et al. first fabricated multi-walled VACNT (MWCNT) membranes with an inner core diameter of ca. 6 nm embedded in a rigid polystyrene matrix [5]. They demonstrated that liquid transport through the MWCNT membrane was several orders of magnitude faster than predictions from the classical hydrodynamics theory [15]. Holt et al. have adopted a micro-fabrication method [6] to produce membranes in which 1.6-nm-wide double-walled CNTs (DWNT) serve as only through-pores spanning a silicon nitride matrix deposited by chemical vapor deposition (CVD). Reported values of liquid and gas flows in DWNTs were several orders of magnitude larger than predicted

* Corresponding author. Tel.: +1 925 423 8021.
E-mail address: kim55@llnl.gov (S. Kim).

http://dx.doi.org/10.1016/j.memsci.2014.02.016
0376-7388

by conventional hydrodynamics and Knudsen diffusion model, respectively. Yu et al. have used a matrix-free approach to fabricate CNT membranes [11]: capillary forces during solvent wetting and evaporation from as-grown CNT arrays produced small-size CNT mats with densities a few orders of magnitude higher than in other CNT membranes. Marand and coworkers developed a scalable, fabrication method, in which a preferential vertical alignment of single-walled CNTs (SWNTs) was achieved during filtration of a SWNT dispersion through a porous membrane, followed by sealing of the inter-SWNT spacing with polysulfone or polyacrylate copolymer [9,16,17]. The prepared SWNT membrane showed a CO_2/CH_4 mixture selectivity differing from the ideal gas selectivity, suggesting non-Knudsen transport through the SWNT interior. In another work, Wu and Hinds [18] have thoroughly mixed bulk nanotubes with epoxy resin and cut the cured CNT/epoxy composite into a 5-μm-thick slice using a microtome. More recently, Mauter et al. have used a magnetic field to orient liquid crystal mesophases of hexagonally packed cylindrical micelles and to template the alignment of SWNTs sequestered in the micellar cores [12].

Table 1 summarizes pros and cons of typical vertically aligned CNT (VACNT) membrane fabrication techniques. Unfortunately, all the CNT membranes produced so far suffer from at least one of the following drawbacks: (1) low density of CNT pores [16,19], (2) only partial CNT vertical alignment [16], (3) a brittle matrix [5,6], (4) rather small membrane active area and long fabrication processes [6], and (5) blocking of a large fraction of the pores by catalyst nanoparticles [19], excess matrix material [9], or polymerization inside the nanochannels [16]. These issues have hampered widespread successful production of CNT/polymer composite membranes that fully exploit the transport properties of the CNT channels. Hence, there still exists an impelling need for the development of defect-free, flexible, large active-area CNT membranes with well-aligned nanotubes and large pore density.

Choices of the polymeric matrix and specific processing steps are crucial for the successful fabrication of such CNT membranes. Liquid-phase processing such as the infiltration of a polymer solution into a CNT array often results in uneven CNT condensation, defects in polymer matrix, and loss of vertical CNT orientation during capillary condensation induced by solvent evaporation (Fig. S1). One promising approach for controlling CNT alignment during the polymer composite fabrication is to infiltrate monomers into the pre-aligned nanotube array, followed by in-situ polymerization [20,21]. By adopting this method here we overcome the typical limitation of polymer solution processes and demonstrate flexible, aligned-CNT/polymer composite membranes having relatively-high density CNTs. In our novel in-situ bulk polymerization method, end-protected vertically-aligned CNT arrays were infiltrated with styrene monomer with a certain amount of polystyrene–polybutadiene (PS-b–PB) block copolymer that acts as a plasticizer. A membrane matrix without larger structural defects obtained in this way combined high surface conformity with tunable flexibility. By adding PS-b–PB, the mechanical properties of the membrane were improved. Scanning electron microscopy (SEM) analysis also confirmed that alignment of CNTs remained undisturbed during the polymerization. These CNTs/polymer composite membranes showed very large gas and water permeabilities similar to those observed from the VACNT membranes reported in literatures [5,6,9,16,19,22], posing great promise in membrane applications that demand high flux, flexibility and durability.

2. Experimental

2.1. Membrane fabrication

The procedure for CNT/polymer composite membrane fabrication is shown in Fig. 1(a). To maintain nanotube alignment during styrene monomer infiltration into CNT mats, a wet PVA (89% hydrolyzed, Sigma-Aldrich) film of ca. 500 μm in thickness was gently attached on the top of CNTs. The assembly was dried under a vacuum to remove any water in the PVA film. The assembled PVA/CNT array was placed between two glass slides with PTFE spacers and the mold was sealed using a 20 wt% PVA solution as glue (Fig. 1(b)). The desired amount of PS-b–PB block copolymer (PS-block–PB-block–PS, styrene 30 wt%, Mw ~ 140,000, Sigma-Aldrich) was dissolved in styrene monomer (Sigma-Aldrich) with magnetic stirring. After 10 h of mixing, 0.5 wt% of 2,2′-azobisisobutyronitrile (Sigma-Aldrich) was added to the styrene monomer and PS-b–PB block copolymer mixture. The prepared mixture was injected into the mold and polymerized at 80 °C for 10 h in an argon-purged oven. Removal of the CNT/polymer composite from the mold could be easily achieved by dissolving PVA in warm water. The composite of polymer and CNT arrays was removed from silicon wafer with a 10 vol% HF solution. A reactive ion etching (RIE) plasma (Samco, RIE-1C), using 4:1 ratio of CF_4/O_2 at 10 W power, was used to clean sample surfaces as well as to open the CNT ends (Fig. 1(c)).

Table 1
Typical vertically aligned CNT membrane techniques reported in the literatures.

CNT	Pore diameter (nm)	Matrix/fabrication method	Density ($\times 10^{10}$ cm^{-2})	Advantages	Disadvantages
Post aligned SWNT [16]	1.2	Polyacrylate copolymer/ in-situ polymerization	0.7	• Scalability	• Low CNT density • Partial CNT alignment • Possible CNT damage during the cutting process
CVD-DWNT [6]	1.6	SiN_x/CVD	25	• Fast flux • Large flux enhancement	• Complicated membrane fabrication process • Poor mechanical properties
CVD-MWNT/alumina [19]	6.3	Polystyrene/solution casting	0.19	• Scalability/simple process	• Low CNT density • Low flux
CVD-MWNT [5]	7.0	Polystyrene/solution casting	6	• Fast flux • Large flux enhancement	• Poor mechanical properties
Carbon pipes [22]	43	CVD deposition of carbon on anodic aluminum oxide	1.07	• Simple process	• Poor mechanical properties • Low flux enhancement

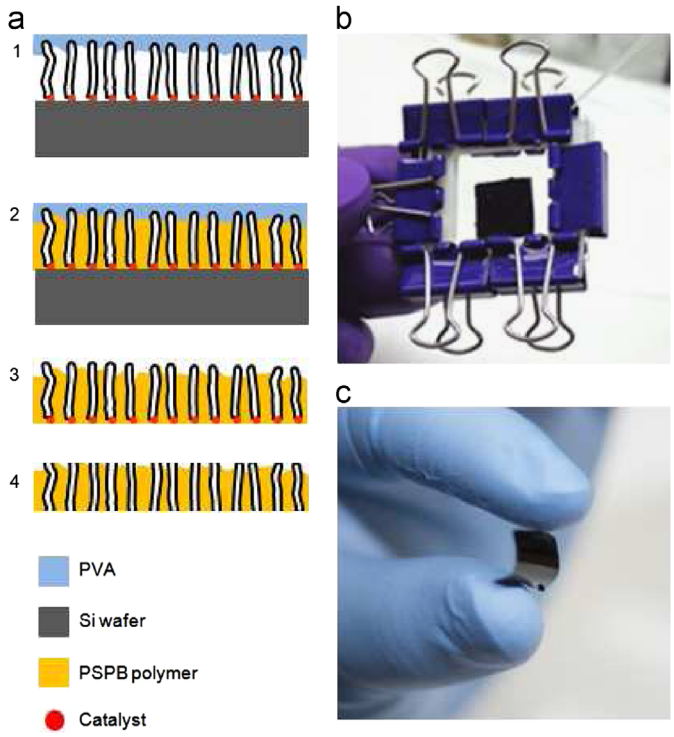

Fig. 1. (a) Fabrication procedure. Step 1: attachment of PVA film on CNT array; 2: in-situ polymerization; 3: PVA film and Si-wafer removal; 4: RIE etching. (b) Polymer solution injection into the mold. (c) Prepared CNT/polymer composite sample.

In this study, performance of CNT/polymer composite membranes was compared directly to the performance of CNT/SiN_x membranes (as a reference membrane) under the same test condition. CNT/SiN_x membranes were fabricated according to the previously reported method [6–8]. Briefly, a VACNT array was grown on a silicon wafer coated with Fe/Mo catalyst *via* CVD using ethylene as the carbon precursor. Low pressure CVD of silicon nitride (SiN_x) filled the inter-nanotube gaps to form a membrane structure. Metallic nanoparticles on one side of the composite were removed by argon ion milling. RIE in oxygen-containing plasma removed the excess SiN_x layer on the other side of the composite and cut open the CNT end tips.

To grow VACNT arrays, we used a 1-in. quartz tube CVD furnace for the CNT/SiN_x membrane fabrication, and a 4-in. wafer-scale, cold-wall furnace reactor (Black Magic, Aixtron) for the polymer/CNT composites membranes. Because of the different matrix infiltrations and CNT membrane fabrication methods, we used VACNT mats with ca. 20–50 μm thickness for the CNT/polymer composite membrane fabrication, whereas 5-μm-thick CNT mats were used for the CNT/SiN_x membrane.

2.2. Membrane characterization

VACNT mats used for membrane fabrication were characterized by micro-Raman (Nicolet Almega XR dispersive Raman spectrometer, Thermo Scientific) spectroscopy and high-resolution transmission electron microscopy (TEM). Gas permeance through the CNT membrane was measured using a constant pressure system equipped with a calibrated mass flow meter. Rejections of 5-nm-diameter colloidal Au nanoparticles (Ted-Pella), 0.5 mM potassium ferricyanide ($K_3Fe(CN)_6$, Sigma-Aldrich) and methylene blue (Sigma-Aldrich) were evaluated by standard permeation tests using a custom-made, stainless-steel dead-end stirred cell designed for the CNT membrane test. The test cell was placed on a magnetic stir plate. The feed side was filled with 10 mL of test solution pressurized by nitrogen. The $K_3Fe(CN)_6$ solutions collected at the permeate side of the CNT membranes were analyzed with UV–vis spectroscopy (Shimadzu UV–vis Spectrometer).

For the evaluation of mechanical properties of the composite membranes, we carried out an indentation test using a universal testing machine. Tests were done with a 1-mm-radius steel ball bearing as an indenter in an universal testing machine described elsewhere [23,24]. The sample films were mounted on a cylinder with an inner diameter of 4.9 mm, using UV curable adhesive. The ball was centered onto the film with a precision of <50 μm and then indented at a rate of 100 μm/min.

3. Results and discussions

For a successful fabrication of CNT membranes several factors are of key importance: (a) use of atomically smooth and well-graphitized CNTs; (b) barrier properties of polymer matrix; (c) easy exposure and opening of the CNT tips; (d) achieving/maintaining vertical orientation of the CNTs while avoiding kinks/bends during fabrication; and (e) mechanical stability.

(a) *Quality of the CNT arrays:* Raman spectra (Fig. 2(b)) collected from the top of a 30-μm-thick VACNT forest (Fig. 2(a)) for polymer/CNT membrane fabrication indicate that the as-grown nanotubes are well-graphitized with a *G* (1595 cm^{-1})-to-*D* (1310 cm^{-1}) band ratio as high as 10 and with a clearly distinguished shoulder peak at 1560 cm^{-1}. Pronounced radial breathing mode suggests a large population of SWNTs and DWNTs. The TEM image shown in Fig. 2(c) clearly confirmed that the as-grown CNTs were SWNT or DWNT with low defect density. CNT inner diameter distribution was measured by analyzing about 30 samples in the TEM image. Fig. 2(d) shows that VACNT arrays with 30 μm thickness have a narrow diameter distribution from 2 to 5 nm with average 3.3 nm. Those used for CNT/SiN_x membrane fabrication were 1–2 nm wide [6]. *G*/*D* ratio of the CNT arrays for the CNT/SiN_x membrane was close to 10 similar to that of CNT array for the polymer/CNT membrane.

(b) *Barrier properties of polymer matrix*: As-synthesized CNT/polymer composite membrane before RIE etching did not show any measurable gas flux through the membrane (detection limit ~0.001 sccm). In addition, we did not see any liquid flux of as-synthesized composite film when using pressures up to 10 bar until the films were cracked at high feed pressure. Only a few minutes of RIE (typically 2–5 min) were sufficient to open the pores of the composite membrane, allowing for preservation of the integrity of the PS/PS-b–PB matrix.

(c) *Access and opening of the CNT tips*: A low and high magnification SEM image of the cross-section of the CNT composite (Fig. 3(a) and (b)) clearly shows that, even before RIE etching, there is no excess polymer layer on the top of the composite film, and that most CNT end tips are protruding out of the composite surface [5,25]. This absence of an excess layer is an important feature of our fabrication method for aligned CNT/polymer composite membranes. Most aligned CNT/polymer composites previously reported by other researchers had a relatively-thick excess polymer layer on the top of the CNT mats [5,20] that needed to be removed by, for example, gentle mechanical polishing, plasma etching, or spin-coating using an organic solvent. These methods require long processing times and sometimes result in damages to the thin composite film. On the contrary, by minimizing any excess polymeric layer our technique requires only short and simple etching for exposing and opening the CNTs to permit fluid flow.

(d) *CNT orientation*: To fully exploit CNT fast mass-transport properties in a membrane, it is also important to avoid bending or kinking of

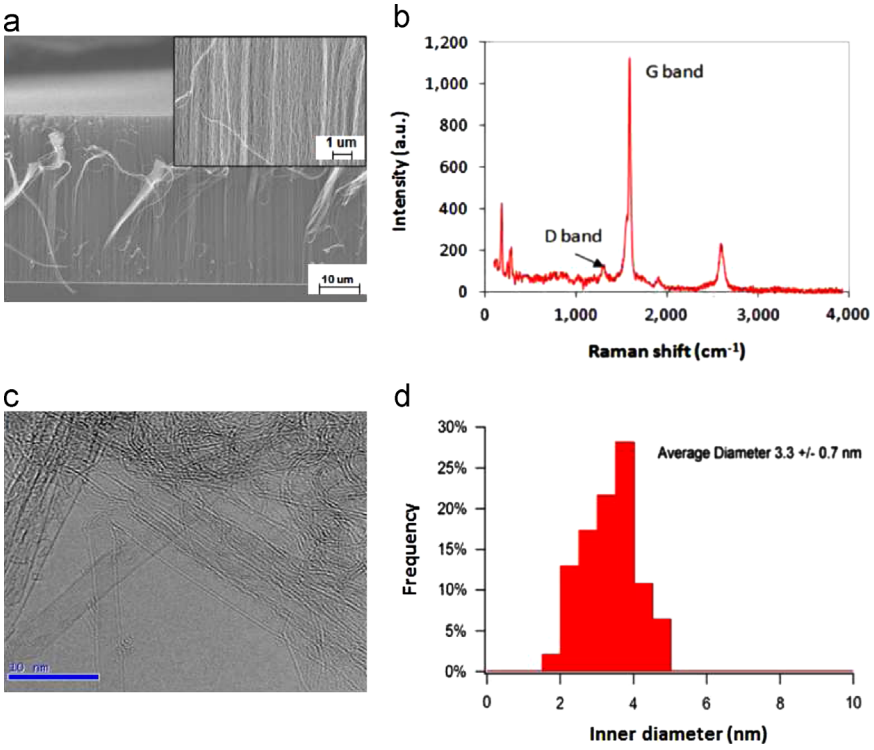

Fig. 2. Characterization of CNT arrays: (a) SEM images of vertically aligned CNT array with 30 μm thickness, (b) Raman spectra for the full 100–3400 cm^{-1} range, (c) a representative TEM image used to determine the CNT diameter distribution, and (d) inner diameter distribution of CNTs determined from (c).

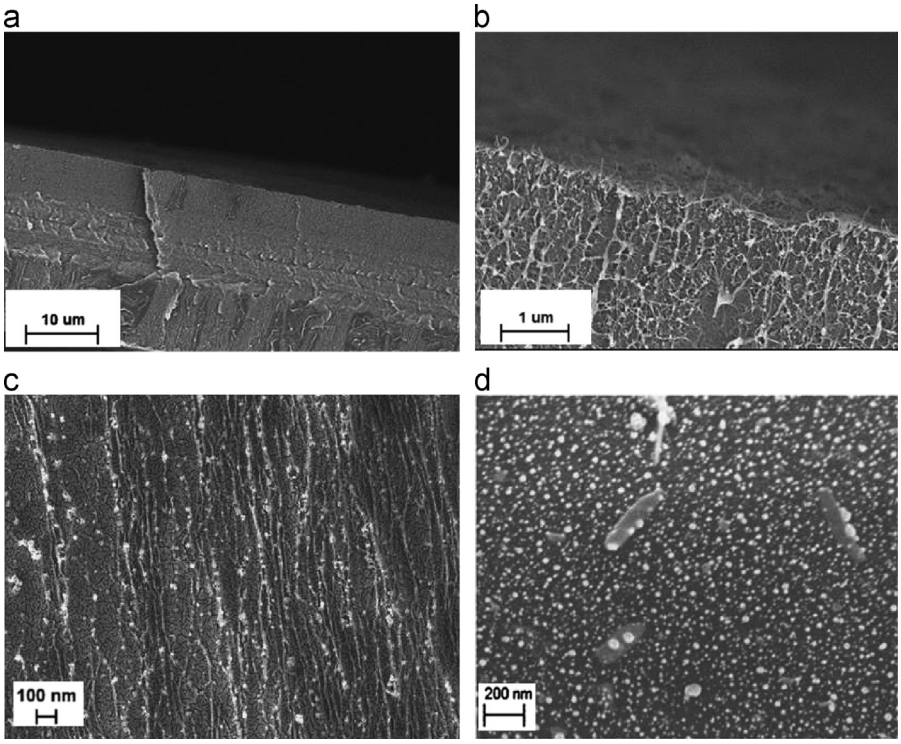

Fig. 3. SEM images: (a) lower magnification, (b) higher magnification showing no excess polymer layer on the top of CNT composites, (c) higher magnification after plasma ethching showing aligned CNTs in polymer matrix and (d) higher magnification of top surface of CNT/polymer membrane.

nanotubes in the polymer matrix during membrane fabrication. Fig. 3(c) shows a cross-sectional view of the sample after mild plasma etching to remove nanotubes that were pulled out of the array during the SEM sample preparation using liquid N_2. This high-magnification SEM image confirms that the CNTs remain well aligned in the polymer matrix.

(e) *Mechanical stability*: Strong and flexible membrane films are desirable for any membrane applications. The mechanical

properties of the CNT/polymer films were measured using a micro-indentation method when PS or PS/PS-b–PB was used as a polymer matrix. It is difficult to measure modulus of the CNT/PS composite film because the CNT/PS samples are too stiff to calculate a modulus with the indentation method. Also, these samples are too brittle to be clamped in a sample loading cell of dynamic mechanical thermal analysis (DMTA) or Instron dynamic and fatigue system and therefore, elastic modulus of the CNT/PS sample is not discussed in this work. However, micro-indentation measurements showed that the addition of 8 wt% PS-b–PB copolymer into the matrix improved the elongation at break of CNT/PS composite film by three times. Moreover, as shown in Fig. 1(c), the CNT/PS composite films prepared with addition of PS-b–PB copolymer as a plasticizer were flexible whereas CNT/PS composite films were quite brittle. The calculated elastic modulus of the CNT/PS/PS-b–PB membrane ranges between 470 and 980 MPa. It is lower than that of the wavy VACNT/epoxy composite (~5 GPa) [26] but higher than the modulus of VACNT/PDMS (~19 MPa) [27], porous PVDF (47–491 MPa) [28] and porous PTFE membrane (30 MPa) demonstrating its mechanical stability as membrane materials [29].

Our membrane characterization that included SEM imaging and measurement of fluid rates and selectivity for gas and liquid mixtures was consistent with having most of the flow going through nanometer-sized pores. Fig. 3(d) – a typical image of the surface of the composite film – shows CNTs embedded in a high-density polymer matrix free of large surface defects or pinholes. The quality of the membrane can also be characterized by measuring gas permeation dependence on the applied feed pressure. In general, gas transport through a porous membrane can be described by viscous flow, Knudsen diffusion, and surface diffusion [30]. Knudsen diffusion occurs when the mean free path of the gas molecules (λ) becomes larger than the membrane pore radius (r). In this condition, collisions of gas molecules with the pore walls are more dominant than molecule–molecule collisions. When r is larger than λ, as in the case for gas transport in pinholes or defects in membrane, intermolecular gas collisions in the viscous flow regime can dominate resulting in loss of gas selectivity. For porous membranes that are governed by Knudsen diffusion, the gas permeance in the Knudsen regime should be independent of the applied feed pressure, whereas it increases with pressure in the viscous regime. Fig. 4(a) shows the nitrogen permeability of CNT/polymer composite membrane at different feed pressures. Measured N_2 permeability through CNT membrane is independent of the applied feed pressures. This result means that there is no viscous flow through any large pinholes or large structural defects that is larger than λ of N_2 at room temperature, ~60 nm. In addition, following example of previous CNT membrane publications [6–8], we tested the prepared membranes for the filtration performance using analytes with small diameter. For these tests, we used 5-nm-diameter Au particles, 0.1 mM Direct Blue 71 (DB71), and 0.5 mM $K_3Fe(CN)_6$ solution (Fig. 4(b)–(d)). As shown in Fig. 4 (b) and (c), permeating solution during filtration of 5 nm Au or DB71 solution through the membrane was clear suggesting complete rejection of the small analytes. In addition, UV–vis spectroscopy analysis showed more than 90% salt rejection when a 0.5 mM $K_3Fe(CN)_6$ solution was used for the filtration tests. As demonstrated previously, CNTs with negatively-charged carboxylate groups at their entrance exhibit significant ion exclusion for salts of multivalent anions and monovalent cations, even if the ion size is somewhat smaller than the CNT diameter [7]. Here, DB71 has four negatively charged sulfonate groups on each monomer side, and its three-axes dimensions are about 3, 1.5, and 1 nm, correspondingly [31]. The reported hydrated radius of $Fe(CN)_6^{3-}$ is around 0.475 nm [7]. Although the average pore size of CNT used in this study is ca. 3 nm and ~10% of the CNTs are 4 nm wide, the presence of carboxylate groups at the CNT pore entrance explains the recorded high rejection for small negatively charged ions. These results also support that the prepared CNT/polymer composite membrane is free of larger defects or pinholes in polymer matrix.

For a successfully fabricated CNT/polymer membrane, we first compared gas and water permeabilities of the CNT/polymer membrane with the reference CNT/SiN_x membrane. As shown in Fig. 5, CH_4, N_2, and water permeabilities are all in narrow range, although there are differences in the exact magnitude of permeabilities. Calculated ideal selectivities of CH_4 over N_2 for CNT/polymer and CNT/SiN_x are 1.48 and 1.51, respectively. These are higher than Knudsen selectivity, 1.32, demonstrating that there is preferential interaction of hydrocarbons with CNTs side walls and that these two CNT membranes have similar gas transport properties. Water transport rates of two CNT membranes are similar although the average pore diameter of CNT array used in CNT/polymer fabrication is about twice that of CNT/SiN_x membrane. Fig. 6 shows the gas permeabilities of the CNT/polymer membrane as a function of the square root of the reciprocal of the molecular weight (i.e., Knudsen model functional dependence on molecular mass) of several tested gases. The mechanism of gas transport through CNT in these conditions is still matter of debate. Previous and our experimental results in this work, however, show that for non-adsorbing gases, such as He and N_2, gas transport scales with molecular weight as predicted by the Knudsen theory [6]. Since CNT membranes have much larger gas permeances than Knudsen model predictions, we scaled up the calculations of flow rates with Knudsen diffusion equation by a factor of 118 to match our experimental data. He and N_2 transport properties of the membrane agree well with the scaled Knudsen diffusion line. On the other hand, the CNT membranes showed higher selectivities for hydrocarbons and CO_2 than expected from Knudsen scaling, suggesting preferential interaction of hydrocarbons and CO_2 with carbon nanotubes. These results are consistent with previously reported data for CNT membranes [6,9].

Following the analysis methods used in previous CNT membrane publications [6–8], we calculated enhancement factors for gas and water as well as corresponding slip lengths of the CNT/polymer membranes. Enhancement factors are shown in Fig. 7. For comparison, we also plotted the enhancement factor and slip length of other CNT membranes [5,6,16,19,22,32], and theoretical estimations [33,34] because we expect gas and water permeabilities in a range similar to that previously recorded for other CNT membranes, thus displaying

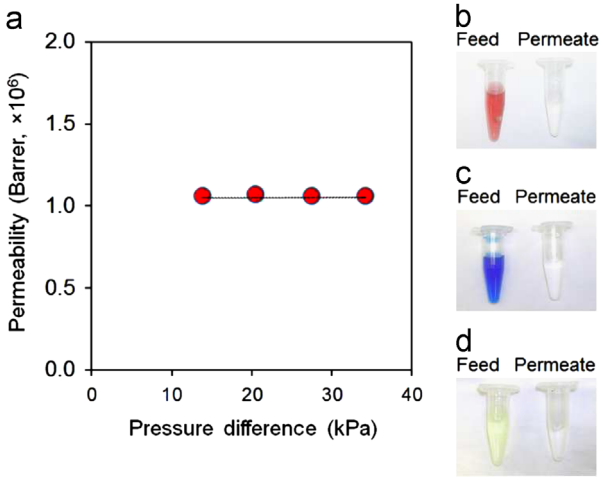

Fig. 4. (a) N_2 permeablity at different feed pressures, (b) 5 nm Au colloid filtration test, (c) 0.1 mM DB71 exclusion test, and (d) 0.5 mM K_4FeCN_6 exclusion test.

analogous enhancement in the fluid transport rates with respect to Knudsen (gas) and Hagen–Poiseuille (water) theories. The accuracy for the calculation could be different for each of the CNT membranes described in the literature because of different fabrication processes and different ways that the number of open nanotubes was determined. While Hinds et al. estimated pore density of the MWNT membrane using KCl diffusion experiment [5,32], a nanotube density estimate of 2.0×10^{11} cm^{-2} of CNT/polymer membrane in this work was calculated with the weight-gain method [35,36]. For CNT/SiN_x membrane, we used the estimate of 2.5×10^{11} cm^{-2} derived from the plain view TEM images of the membrane [6]. Thus, our calculation for enhancement factor and slip length is lower boundary estimates because actual open number of nanotube for mass transport could be lower than our number estimated from the weight-gain method and TEM images analysis. The SWNT membrane of Marand et al. [16], the MWNT membrane of Lin et al. [19], and the carbon pipes membrane of Quirke et al. [22] estimated nanotube density using SEM images and we hypothesize their numbers are also lower boundary estimates similar to the pore density estimation in this work. Fig. 7(a) shows calculated enhancement factors for gas. Because the mean free path of N_2 at room temperature ($\lambda\sim60$ nm) is significantly larger than the pore diameter of our membrane ($d=3.3$ nm), we have calculated the enhancement factor for N_2 based on the theoretical Knudsen model.

By assuming negligible contribution of surface flow of N_2 to the total flow, the gas flow rate can be expressed by the Knudsen equation:

$$J_{Kn}=\frac{2}{3}\sqrt{\frac{8\pi}{MRT}}\left(\frac{d}{2}\right)^3 V_m\frac{\Delta P}{L}\sigma A \tag{1}$$

where M is the molecular weight, R is the universal gas constant, T is the absolute temperature, d is the pore diameter, V_m is the molar volume, ΔP is the pressure drop, L is the thickness of the membrane, σ is the areal DWNT density, and A is the test area of the membrane. The gas-flow enhancement is consistent with the atomistic simulations discussed above and the previous experimental observations of Hinds et al.[5,32] and Holt et al. [6]. Interestingly, Fig. 7(a) shows that N_2 enhancement factors of the CNT membranes prepared using the CVD process and the plasma etching process are similar although tube length/diameter, and the membrane fabrication methods are different. Although the CNT/PS membrane prepared by Lin et al. [19] used the direct CVD growth of VACNT array, it shows lower enhancement factor possibly due to remained catalyst particles on the bottom of CNT tips embedded in polystyrene and alumina membrane support. The SWNT membrane prepared using the post-CNT alignment method also shows low enhancement factor similar to Lin et al.'s measurement [19]. We hypothesize that the low value of the SWNT membrane is due to partial nanotube alignments and defects on the tube wall generated during the cutting process.

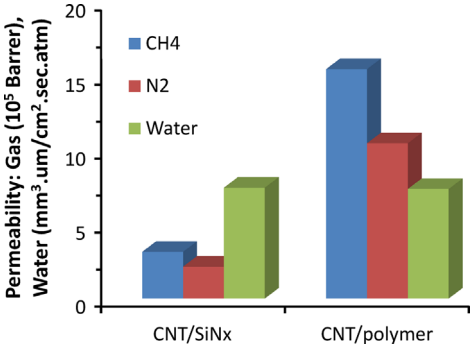

Fig. 5. Gas and water permeabilities of CNT/polymer and CNT/SiN_x membranes.

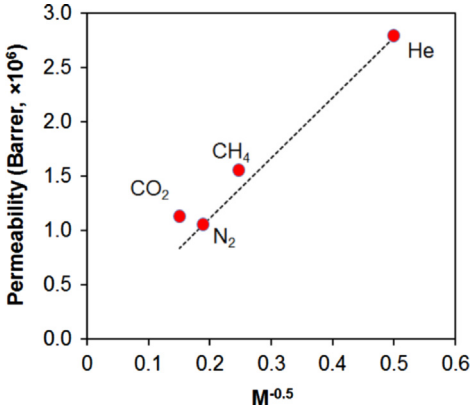

Fig. 6. Single-gas permeability as a function of the inverse square root of the molecular weight of the penetrant.

Following previous literature and extrapolating its validity to nanoscale, we used the Hagen–Poiseuille equation with the inclusion of a slip-flow correction to estimate the volumetric flow rate Q_{SLIP} of water through long cylindrical pores:

$$Q_{SLIP}=\frac{\pi}{8\mu}\left[\left(\frac{d}{2}\right)^4+4L_s\left(\frac{d}{2}\right)^3\right]\frac{\Delta P}{L}, \tag{2}$$

where μ is the water viscosity, and L_s is defined as the slip length:

$$L_s=\frac{U_{wall}}{dU/dr}, \tag{3}$$

where U_{wall} is the axial velocity at the wall, and dU/dr is the radial velocity gradient at the wall.

In Fig. 7(b) and (c), we present the enhancement factor and slip length of CNT/polymer membrane for water. The results of CNT/polymer membrane are comparable to the CNT/SiN_x membrane [6,7]. Contrary to the results of gas transport through CNTs, the values of the CNT/polymer membrane are lower than that of 1.6 nm diameter CNT/SiN_x membrane and ~7 nm diameter MWNT/PS membrane. However, the CNT/polymer membrane shows higher enhancement factor than 43 nm carbon nanopipes membranes by Quirke et al. [22]. Although there are uncertainties in estimation of areal nanotube density in each CNT membranes, the result suggests that the enhancement factor decreases with increasing tube diameter except the MWNT membrane by Hinds et al. [5,32]. In addition, these trends are consistent with molecular dynamics simulation studies of McGaughey et al., which suggest that the flow enhancement factor and slip length are dependent on CNT diameter [33,34]. The water transport phenomena are more sensitive to the nature of CNTs and the membrane fabrication method. Several molecular dynamics simulation studies have shown that the basic gas transport mechanism underlying the appearance of rapid diffusion in CNT pores is not strongly dependent on their diameter and length because gas molecules travel mostly near the CNT surface rather than moving ballistically across the pore [37,38]. On the contrary, molecular dynamics simulation study for water transport through CNT suggested that slip length increases with decreasing CNT diameter because curvature induced effects weaken the coupling between water molecules and the CNT wall [34]. Indeed, a curved surface pinches the low-energy potential wells and squeezes water molecules away from CNT surface, thus enhancing water flow rate and slip length. However, besides tube diameter, tube length, tortuosity, and chirality could be other important parameters which can affect fluid transport through CNTs.

4. Conclusions

Flexible, robust, and large-area membranes having VACNT arrays as pores were prepared by a novel in-situ polymerization method that prevents pore blocking and perturbation of nanotube

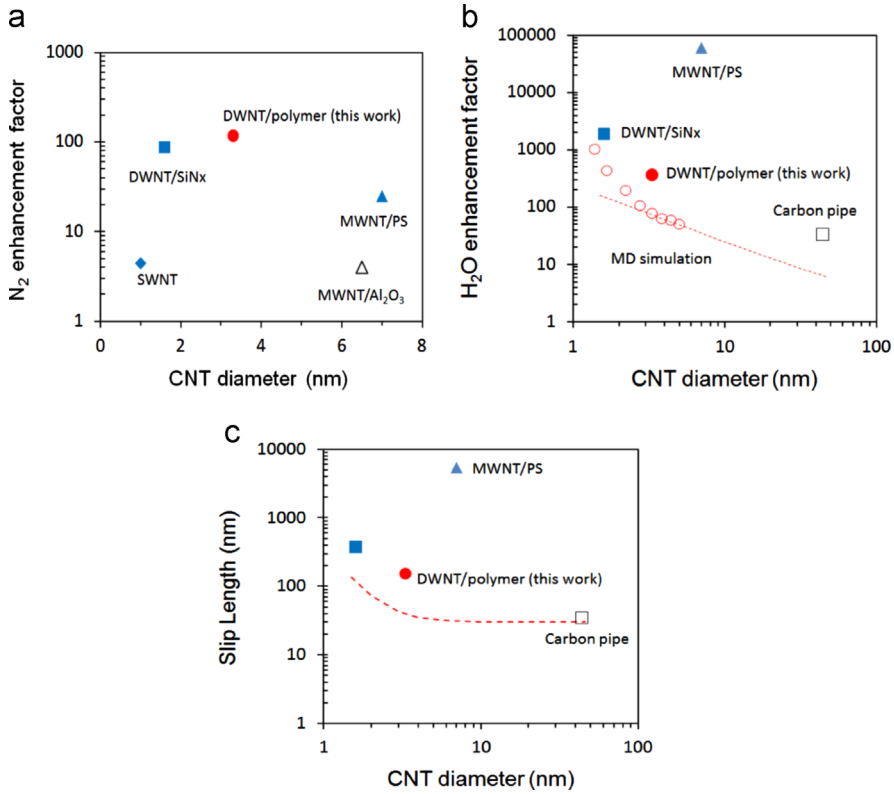

Fig. 7. Calculated (a) enhancement over Knudsen model, (b) enhancement over no-slip, hydrodynamic model, and (c) slip length. (■) DWNT/SiN_x membrane [6]; (●) DWNT/polymer membrane [this work]; (♦) post aligned SWNT membrane [16]; (▲) CVD-MWNT/PS membrane [5]; (△) CVD-MWNT/Al_2O_3 membrane [19]; (▫) carbon pipe membrane [22]; (○,—) MD simulation [33,34].

alignment. Well-graphitized, vertical arrays of CNTs were infiltrated with a mixture of styrene monomer with a certain amount of polystyrene–polybutadiene (PS-b–PB) block copolymer that acts as a plasticizer. The VACNT/PS composite membrane with addition of PS-b–PB copolymer was flexible whereas VACNT/PS membrane was quite brittle. Microindentation measurements confirmed that the addition of PS-b–PB copolymer into the matrix improved the elongation at break of VACNT/PS film. SEM images showed that well aligned CNTs were embedded in a high-density polymer matrix free of any macroscopic voids or structural defects. Measured selectivity for gas and liquid mixtures using DB71, $K_3Fe(CN)_6$, or 5-nm Au particles also verified high quality of the CNT/polymer composite membrane. The gas and liquid transport properties of these VACNT/polymer composite membranes were comparable to that of other VACNT membranes reported in the literatures, demonstrating successful fabrication of flexible, VACNT/polymer composite membranes.

The CNT membranes in this study have gas selectivities that approach Knudsen selectivities and low salt rejection because the average pore size of the membranes is larger than 3 nm. However, their gas selectivities or ion rejection could be enhanced by surface functionalization. The tips of open CNTs are decorated with carboxylate groups that are an easy target for further modification of CNT membranes with specific chemical groups via various conventional functionalization methods such as zwitterion reaction [17] or carbodiimide coupling reaction [39]. We used VACNT mats with ca. 20–50 μm thickness for the fabrication of free-standing VACNT/polymer composite membrane; however, it is possible to make a thinner CNT/polymer composite membrane if the CNT/polymer composite film is transferred and supported on the membrane support (e.g. microporous membrane). These VACNTs/polymer membranes potentially enable applications that may require membranes with high flux, high selectivities, flexibility, and durability.

Acknowledgments

This work was partially supported by NSF NIRT CBET-0709090. Lawrence Livermore National Laboratory is operated by Lawrence Livermore National Security, LLC, for the U.S. Department of Energy, National Nuclear Security Administration under Contract DE-AC52-07NA27344. C. Grigoropoulos, O. Bakajin, and S. Kim acknowledge support by NSF NIRT CBET-0709090. H.G. Park acknowledges support by Swiss National Science Foundation (Contract no. 200021-137964).

Appendix A. Supplementary information

Supplementary data associated with this article can be found in the online version at http://dx.doi.org/10.1016/j.memsci.2014.02.016.

References

[1] J. Kong, N.R. Franklin, C. Zhou, M.G. Chapline, S. Peng, Kyeongjae Cho, H. Dai, Nanotube molecular wires as chemical sensors, Science 28 (2000) 622–625.
[2] P.G. Collins, K. Bradley, M. Ishigami, A. Zettl, Extreme oxygen sensitivity of electronic properties of carbon nanotubes, Science 287 (2000) 1801–1804.
[3] P. Calvert, Nanotube composites: a recipe for strength, Nature 399 (1999) 210.
[4] J.M. Planeix, N. Coustel, B. Coq, V. Brotons, P.S. Kumbhar, R. Dutartre, P. Geneste, P. Bernier, P.M. Ajayan, Application of carbon nanotubes as supports in heterogeneous catalysis, J. Am. Chem. Soc. 116 (1999) 7935–7936.
[5] B.J. Hinds, N. Chopra, T. Rantell, R. Andrews, V. Gavalas, L.G. Bachas, Aligned multiwalled carbon nanotube membranes, Science 303 (2003) 62–65.
[6] J.K. Holt, H.G. Park, Y. Wang, M. Stadermann, A.B. Artyukhin, C.P. Grigoropoulos, A. Noy, O. Bakajin, Fast mass transport through sub-2-nanometer carbon nanotubes, Science 312 (2006) 1034–1037.

[7] F. Fornasiero, H.G. Park, J.K. Holt, M. Stadermann, C.P. Grigoropoulos, A. Noy, O. Bakajin, Ion exclusion by sub-2-nm carbon nanotube pores, Proc. Natl. Acad. Sci. USA 105 (2008) 17250–17255.
[8] F. Fornasiero, J. Bin In, S. Kim, H.G. Park, Y. Wang, C.P. Grigoropoulos, A. Noy, O. Bakajin, pH-tunable ion selectivity in carbon nanotube pores, Langmuir 26 (2010) 14848–14853.
[9] S. Kim, J.R. Jinschek, H. Chen, D.S. Sholl, E. Marand, Scalable fabrication of carbon nanotube/polymer nanocomposite membranes for high flux gas transport, Nano Lett. 7 (2007) 2806–2811.
[10] W. Mi, Y.S. Lin, Y. Li, Vertically aligned carbon nanotube membranes on macroporous alumina supports, J. Membr. Sci. 304 (2007) 1–7.
[11] M. Yu, H.H. Funke, J.L. Falconer, R.D. Noble, High density, vertically-aligned carbon nanotube membranes, Nano Lett. 9 (2009) 225–229.
[12] M.S. Mauter, M. Elimelech, C.O. Osuji, Nanocomposites of vertically aligned single-walled carbon nanotubes by magnetic alignment and polymerization of a lyotropic precursor, ACS Nano 4 (2010) 6651–6658.
[13] G. Hummer, J.C. Rasaiah, J.P. Noworyta, Water conduction through the hydrophobic channel of a carbon nanotube, Nature 414 (2001) 188–190.
[14] A.I. Skoulidas, D.M. Ackerman, J.K. Johnson, D.S. Sholl, Rapid transport of gases in carbon nanotubes, Phy. Rev. Lett. 89 (2002) 185901–185904.
[15] M. Majumder, N. Chopra, R. Andrews, B.J. Hinds, Nanoscale hydrodynamics: enhanced flow in carbon nanotubes, Nature 438 (2005) 44.
[16] A. Surapathi, J. Herrera-Alonso, F. Rabie, S. Martin, E. Marand, Fabrication and gas transport properties of SWNT/polyacrylic nanocomposite membranes, J. Membr. Sci. 375 (2011) 150–156.
[17] W.F. Chan, H.Y. Chen, A. Surapathi, M.G. Taylor, X.H. Hao, E. Marand, J. K. Johnson, Zwitterion functionalized carbon nanotube/polyamide nanocomposite membranes for water desalination, ACS Nano 7 (2013) 5308–5319.
[18] J. Wu, K.S. Paudel, C. Strasinger, D. Hammell, A.L. Stinchcomb, B.J. Hinds, Programmable transdermal drug delivery of nicotine using carbon nanotube membranes, Proc. Natl. Acad. Sci. USA 107 (2010) 11698–11702.
[19] W. Mi, Y.S. Lin, Y. Li, Vertically aligned carbon nanotube membranes on macroporous alumina supports, J. Membr. Sci. 304 (2007) 1–7.
[20] N.R. Raravikar, L.S. Schadler, A. Vijayaraghavan, Y.P. Zhao, B.Q. Wei, P. M. Ajayan, Synthesis and characterization of thickness-aligned carbon nanotube-polymer composite films, Chem. Mater. 17 (2005) 974–983.
[21] H. Huang, C.H. Liu, Y. Wu, S.S. Fan, Aligned carbon nanotube composite films for thermal management, Adv. Mater. 17 (2005) 1652.
[22] M. Whitby, L. Cagnon, M. Thanou, N. Quirke, Enhanced fluid flow through nanoscale carbon pipes, Nano Lett. 8 (2008) 2632–2637.
[23] S.O. Kucheyev, M. Stadermann, S.J. Shin, J.H. Satcher, S.A. Gammon, S.A. Letts, T. van Buuren, A.V. Hamza, Super-compressibility of ultralow-density nanoporous silica, Adv. Mater. 24 (2012) 776.
[24] M.R. Begley, T.J. Mackin, Spherical indentation of freestanding circular thin films in the membrane regime, J. Mech. Phys. Solid 52 (2004) 2005–2023.
[25] M. Kang, S.J. Myung, H.J. Jin, Nylon 610 and carbon nanotube composite by in situ interfacial polymerization, Polymer 47 (2006) 3961–3966.
[26] H. Cebeci, R.G.d. Villoria, A.J. Hart, B.L. Wardle, Multifunctional properties of high volume fraction aligned carbon nanotube polymer composites with controlled morphology, Compos. Sci. Technol. 69 (2009) 2649–2656.
[27] L. Ci, J. Suhr, V. Pushparaj, X. Zhang, P.M. Ajayan, Continuous carbon nanotube reinforced composites, Nano Lett. 7 (2008) 2762–2766.
[28] C. Feng, B. Shi, G. Li, Y. Wu, Preparation and properties of microporous membrane from poly(vinylidene fluoride-co-tetrafluoroethylene) (F2.4) for membrane distillation, J. Membr. Sci. 237 (2004) 15–24.
[29] W.-C. Ko, C.-K. Tseng, W.-J. Wu, C.-K. Lee, Charge storage and mechanical properties of porous PTFE and composite PTFE/COC electrets, E-Polymers 32 (2010).
[30] R.J.R. Uhlhorn, K. Keizer, A.J. Burggraff, Gas and surface diffusion in modified r-alumina systems, J. Membr. Sci. 46 (1989) 225–241.
[31] T.-Z. Ren, Z.-Y. Yuan, B.-L. Su, Encapsulation of direct blue dye into mesoporous silica-based materials, Colloids Surf. A 300 (2007) 79–87.
[32] M. Majumder, N. Chopra, B.J. Hinds, Mass transport through carbon nanotube membranes in three different regimes: Ionic diffusion and gas and liquid flow, ACS Nano 5 (2011) 3867–3877.
[33] J.A. Thomas, A.J.H. McGaughey, Reassessing fast water transport through carbon nanotubes, Nano Lett. 8 (2008) 2788–2793.
[34] J.A. Thomas, A.J.H. McGaughey, Water flow in carbon nanotubes: transition to subcontinuum transport, Phys. Rev. Lett. 102 (2009) 184502.
[35] G. Zhong, J.H. Warner, M. Fouquet, A.W. Robertson, B. Chen, J. Robertson, Growth of ultrahigh density single-walled carbon nanotube forests by improved catalyst design, ACS Nano 6 (2012) 2893–2903.
[36] S. Esconjauregui, R. Xie, M. Fouquet, R. Cartwright, D. Hardeman, J. Yang, J. Robertson, Measurement of area density of vertically aligned carbon nanotube forests by the weight-gain method, J. Appl. Phys. 113 (2013).
[37] A.I. Skoulidas, D.S. Sholl, J.K. Johnson, Adsorption and diffusion of carbon dioxide and nitrogen through single-walled carbon nanotube membranes, J. Chem. Phys. 124 (2006) 054708.
[38] H. Chen, J.K. Johnson, D.S. Sholl, Transport diffusion of gases is rapid in flexible carbon nanotubes, J. Phys. Chem. B. 110 (2006) 1971–1975.
[39] M. Majumder, N. Chopra, B.J. Hinds, Effect of tip functionalization on transport through vertically oriented carbon nanotube membranes, J. Am. Chem. Soc. 127 (2005) 9062–9070.